

## A hysteretic model for the rotational response of embedded column base connections



Pablo Torres-Rodas<sup>a</sup>, Farzin Zareian<sup>a</sup>, Amit Kanvinde<sup>b,\*</sup>

<sup>a</sup> Department of Civil and Environmental Engineering, University of California, Irvine, CA 92697, USA

<sup>b</sup> Department of Civil and Environmental Engineering, University of California, Davis, CA 95616, USA

### ARTICLE INFO

#### Keywords:

Embedded base connections

Steel moment frames

Steel connections

### ABSTRACT

Embedded Column Base (ECB) connections are commonly used in mid- and high-rise steel moment frames, to connect the steel column to the concrete footing. Although recent research has shown these connections to be highly ductile, they are typically designed to be stronger than the adjoining column, resulting in significant cost. To enable assessment of strong-column-weak-base systems that leverage the inherent ductility of these connections, an approach is presented to simulate their hysteretic and dissipative response. The proposed approach simulates ECB connections as an arrangement of two springs in parallel, to reflect moment contributions due to horizontal and vertical bearing stresses. This is informed by recent work that provides physical insight into the internal force transfer within these connections. The springs' response is defined by the pinched Ibarra-Medina Krawinkler (IMK) hysteretic model, which is able to capture both in-cycle and cyclic degradation in strength and stiffness. The model is shown to reproduce the response of ECB connections with reasonable accuracy. Guidelines to calibrate model parameters are presented; these include physics-based estimation of selected parameters such as strength and stiffness, accompanied by empirical calibration of ancillary parameters associated with cyclic deterioration. Limitations are discussed.

### 1. Introduction

Column base connections in steel moment frames may be classified as of the exposed or embedded type. Exposed base plate connections (such as the one shown in Fig. 1a) are common in low-rise (1–3 story) moment frame buildings, where the base moment, shear, and axial force demands are relatively modest. These are less preferable for mid- or high-rise moment frames, since the higher moment demands necessitate a large number of deeply embedded anchor rods and/or thick base plates. In these cases, Embedded Column Base (ECB) connections, such as the one shown in Fig. 1b are more preferable. These connections resist base moments and forces through a combination of bearing stresses on the column flanges and the embedded base plate. Besides, exposed base plate connections may be shallowly embedded under a slab-on-grade cast on top of the base plate. This shallow embedment (typically less than 300 mm) increases the strength and stiffness of the connection.

Exposed base plate connections are well-researched, with validated models for strength (Drake, and Elkin [1]), stiffness (Kanvinde et al. [2], Trautner et al. [3]), component hysteretic response (Torres-Rodas et al. [4]), and methods for design (Fisher and Kloiber [5], Gomez et al.

[6]). In contrast, ECB connections (constructed as per US practice) have attracted research attention only recently; this work includes some of the first experiments on deeply embedded column bases (Grilli et al. [7]), and shallowly embedded column bases (Barnwell [8]). These experiments have led to validated strength models and design methods (Grilli and Kanvinde [9] for deeply embedded, and Barnwell [8] for shallowly embedded), as well as stiffness characterization approaches (Torres-Rodas et al. [10] for deeply embedded, and Tyron [11] for shallowly embedded). A secondary finding of these studies is that ECB connections are ductile (rotation capacity in the range of 0.03–0.08 rad) for the specimens tested by Grilli and Kanvinde [9], and Barnwell [8], even when not explicitly detailed for ductility. In seismic regions, where ECB connections are generally designed to remain elastic (AISC [12]), making this finding to be important. More specifically, ECB connections (and more generally, column base connections in seismic moment frames) are designed to resist a moment equal to  $1.1R_y M_p$  of the connected column (i.e., a “strong-base-weak-column design”). This is based on the presumption that a plastic hinge within the column section (usually a wide-flange cross-section) possesses greater rotation capacity compared to the base connection. This is problematic for two reasons:

\* Corresponding author.

E-mail address: [kanvinde@ucdavis.edu](mailto:kanvinde@ucdavis.edu) (A. Kanvinde).

**Notation**

$\alpha$  Fraction of the moment applied and resisted by vertical bearing mechanism

$a_{pinch}, \Lambda_{K_I}, \Lambda_{M_{peak}}, F_{pr}$  ECB hysteretic parameters

$\beta_i$  Cyclic deterioration parameter

$B$  Base plate width perpendicular to plane of lateral loading

$C$  Constant defining interaction of column with concrete

$c, c_{K_I}, c_{M_{peak}}$  Rate of deterioration parameters (equal to one in all cases)

$d_{embed}$  Embedment depth

$d_{ref}$  Depth at which horizontal bearing stresses attenuate to zero

$d\theta_p, \theta_p$  Plastic rotation

$\epsilon \in \epsilon_u \in \epsilon_c$  Error function, Error function for unconstrained and constrained calibration

$E_{concrete}, E_{steel}$  Modulus of Elasticity of Concrete, Steel

$E_i, E^T$  Energy dissipated at cycle “i”, Reference Energy

$I_i, I_{i-1}$  Values of generic quantity during cycle  $i$  and  $i - 1$

$K_I^{initial}, K_{I,VB}^{initial}, K_{I,HB}^{initial}$  Initial Elastic Stiffness, Vertical spring, Horizontal spring

$I_{column}$  Moment of inertia of embedded column

$M_{base}, M_p$  Base moment, Nominal plastic flexural strength

$M_{FHB}, M_{VB}$  Moment resisted through horizontal bearing, and vertical bearing

$M_y, M_y^+, M_y^-$  Moment at first yield of connection, Moment at first yield in the forward direction, Moment at first yield in the reverse direction

$M_{peak}, M_{peak,HB}, M_{peak,VB}$  Peak moment of the connection, Peak moment of horizontal bearing spring, Peak moment of vertical bearing spring

$M_{test}, M_{MODEL}$  Moment obtained from the test, and model

$N$  Base plate length in the direction of loading

$\theta_{peak}$  Rotation at peak strength of the connection

$R, \Omega_o$  Seismic response modification factor, System overstrength factor

$R_y$  Ratio of the expected yield stress to the specified minimum yield stress

$s_p, M_{max}$  Rotation at which elastic unloading hits horizontal axis, Maximum Moment from previous excursion

$t_p$  Thickness of Base plate at bottom of the column

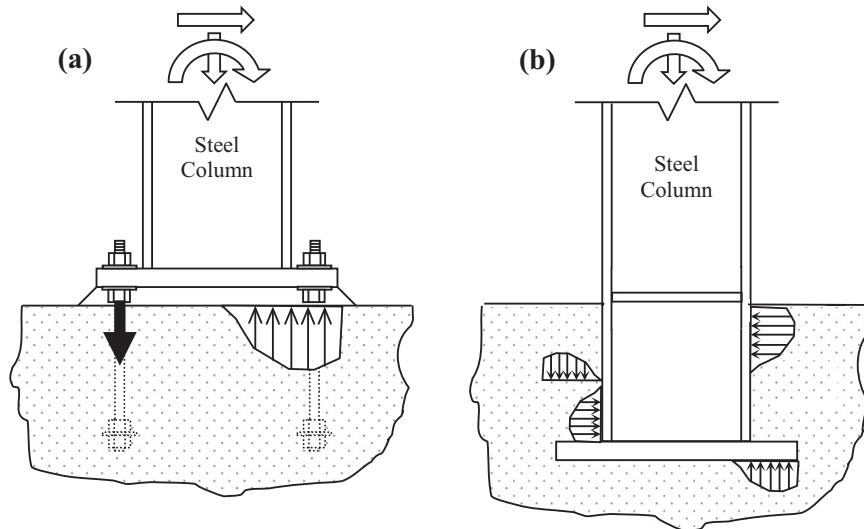


Fig. 1. Types of column base connections: (a) exposed base plate connection with forces resisted by vertical bearing and anchor rod tension, (b) embedded column base, with forces resisted by horizontal bearing stress on column flanges, and vertical bearing stresses on embedded plate.

- From a mechanistic standpoint, the strong-base-weak-column design may not provide superior performance, since the column plastic hinges themselves may have lower rotation capacity (influenced by local and lateral torsional buckling) than the base connections, as determined from experimental data curated by Lignos and Krawinkler [13]. In contrast, the rotational capacity of the base connections referenced above is comparable to that of beam-column moment connections (FEMA 350 [14]), which are the designated “fuse” element in steel moment frames.
- From a constructional standpoint, requiring the base connection to be stronger than the column is expensive, requiring deep embedment, thick embedded base plates, and logistical overhead in terms of multi-stage concrete installation.

In summary, the current design methodology may well be counterproductive, disregarding the deformation capacity of the base connections to promote inelastic action in the columns, resulting in inferior performance at increased costs. Retrospectively, the prevalence of the strong-base-weak-column paradigm may be attributed to the notion that column hinges are likely to be more ductile than base connections,

in the absence of test data to indicate the contrary. A collateral outcome of the strong-base-weak-column paradigm is that the post-yield or hysteretic response of column bases has remained virtually unexamined, since they are designed to remain elastic. Consequently, an approach to simulate hysteretic response of ECB connections is not available within prospective weak-base-strong-column systems that leverage the ductility and dissipative characteristics of base connections. More specifically, hysteretic models for ECB connections are not available for use within nonlinear time history simulations that establish interrelationships between base connection strength, ductility, and system performance. Such simulations (e.g., as outlined in FEMA-P695 [15] and NEHRP [16]) may be used to quantify frame performance metrics such as acceptable response modification factors (i.e.,  $R$  &  $\Omega_o$ ), deformation demands, and probabilities of collapse and their relationship to base connection design.

Within this context, the main objective of this paper is to present a validated method to represent the hysteretic response of ECB connections. The method integrates physical behavior with previously developed models for strength and stiffness, to provide generalized modeling guidelines that effectively represent various aspects of ECB response.

These aspects include the monotonic backbone with yielding and hardening, as well features pertaining to cyclic hysteresis and progressive damage, such as pinching, and strength/stiffness degradation. The next section outlines physical phenomena that control the response and failure modes of the ECB connections. This is followed by description of the proposed modeling approach which decomposes the response into the mechanisms of horizontal and vertical resisting stresses and represents each through a hysteretic model (Ibarra et al., [17]). The paper then describes calibration of this approach based on physical insight and previously developed strength and stiffness models. The response, as obtained from the approach calibrated against these guidelines is then examined against experimental response from five full-scale tests on deeply embedded column base connections conducted by Grilli and Kanvinde [18]. The paper concludes by summarizing limitations of the proposed approach.

## 2. Physical response of connections

Fig. 2a shows a typical moment-rotation response of an ECB connection (tested by Grilli and Kanvinde [18]), whereas Fig. 2b and c show photographs of limit states corresponding to horizontal bearing (i.e. concrete crushing on compression side, gap opening and tension side, and shear cracking in concrete panel), and vertical bearing (i.e. showing visible concrete uplift and corresponding horizontal crack), respectively. The response of all tested connections conducted by Grilli and Kanvinde [7] shows similar characteristics (e.g. pinching behavior, cyclic deterioration) with minor variations depending on the embedment depth (e.g. strength of the connection, rate of deterioration). Fig. 3a–f schematically illustrate the physical response of ECB connections subjected to cyclic loads. The inset graphics represent the evolution of the hysteretic load deformation curve (i.e. lateral load applied at the top of the column multiplied by the lever arm measured as the distance between the load and the top of the concrete pedestal, denoted as base moment  $M$ ; and chord rotation,  $\theta$ ). Referring to Fig. 3, the hysteretic response exhibits the following phases:

1. Phase 1 (Fig. 3a): The first phase corresponds to the initial linear elastic response. Even though small cracks in the concrete foundation are observed near the corners of the column, they do not affect the load deformation response. The applied loads are resisted by a combination of bearing stresses between the column flange and concrete foundation as well as the base plate located at the bottom of the column and the foundation.
2. Phase 2 (Fig. 3b): The linear elastic portion of response ends with a significant loss in stiffness, due to concrete in the bearing zone achieving peak strength. Subsequent to this, a small gap opens between the column flange and the foundation on the tension side. The load deformation response continues with initiation of concrete spalling due to bearing stresses in the column flange (i.e. compression side). The connection strength plateaus when concrete ahead of the column flange begins to crush, accompanied by an increase in

the gap between the tension flange of the column and the surrounding. This type of response continues until one of the following occurs: (1) uplift of a concrete cone on the tension side – discussed later, or (2) load reversal, and unloading – Fig. 3c.

3. Phases 3-4-5-6 (Fig. 3c-d-e-f): Loading in the reversed direction initially has low stiffness, as the column moves within the “pocket” it has created during loading in the forward direction (Fig. 3c). Once the gap is closed (Fig. 3d), the stiffness increases abruptly resulting in “pinched” hysteretic response (Fig. 3e). Subsequent to this re-engagement, response in the reverse direction is similar to that in the forward direction, i.e., elastic loading followed by concrete crushing and a plateau (Fig. 3f).
4. Phases 7–8 (Fig. 3g-h): These correspond to reloading in the forward direction. Qualitatively, this is similar to loading during the first cycle in addition to pinched response due to closure of the gap between the column flange and footing (now in the forward direction – Fig. 3g). Notwithstanding this, various quantities, including strength and reloading stiffness show degradation – Fig. 3h. This degradation may be attributed to progressive crushing or spalling of the concrete in the previous cycle, which leads to reduction of the effective lever arm between the bearing stress blocks on the column flanges. This type of degradation in the moment carrying capacity of the horizontal bearing stresses leads to the gradual transfer of base moment to the embedded base plate (Grilli and Kanvinde [18]), ultimately leading to concrete blowout or uplift failure due to vertical stresses generated by the embedded plate – as shown in Fig. 2c. If sufficient embedment is provided, this type of failure may not occur until significant rotation is reached.

Grilli and Kanvinde [18] postulated physical mechanisms for the internal force transfer in ECB connections, subsequently incorporating these (Grilli and Kanvinde [7]) into a quantitative strength model. As per this model, the base moment is shared by two mechanisms, shown in Fig. 4: (1) horizontal bearing stresses on the column flange acting in conjunction with panel zone shear – Fig. 4a, and (2) vertical bearing stresses that restrain rotation of the embedded base plate – Fig. 4b. Further, Grilli and Kanvinde [7] propose that prior to failure due to horizontal bearing stresses (e.g., concrete spalling ahead of column flange), the distribution of moment between these two mechanisms bears a constant ratio, dependent on the embedment depth. Specifically, moments supported by vertical and horizontal bearing stresses may be estimated as follows:

$$M_{VB} = \alpha \times M_{base} \tag{1}$$

and,

$$M_{HB} = (1 - \alpha) \times M_{base} \tag{2}$$

In the above equations,  $M_{base}$  is the total base moment, whereas the ratio  $\alpha$  controls the relative contribution of the two mechanisms. The ratio itself is dependent on the embedment depth, such that the share of the moment carried by horizontal bearing increases as the embedment



Fig. 2. Response of ECB: (a) Moment Rotation Response, (b) bearing cracking, (c) uplift failure.

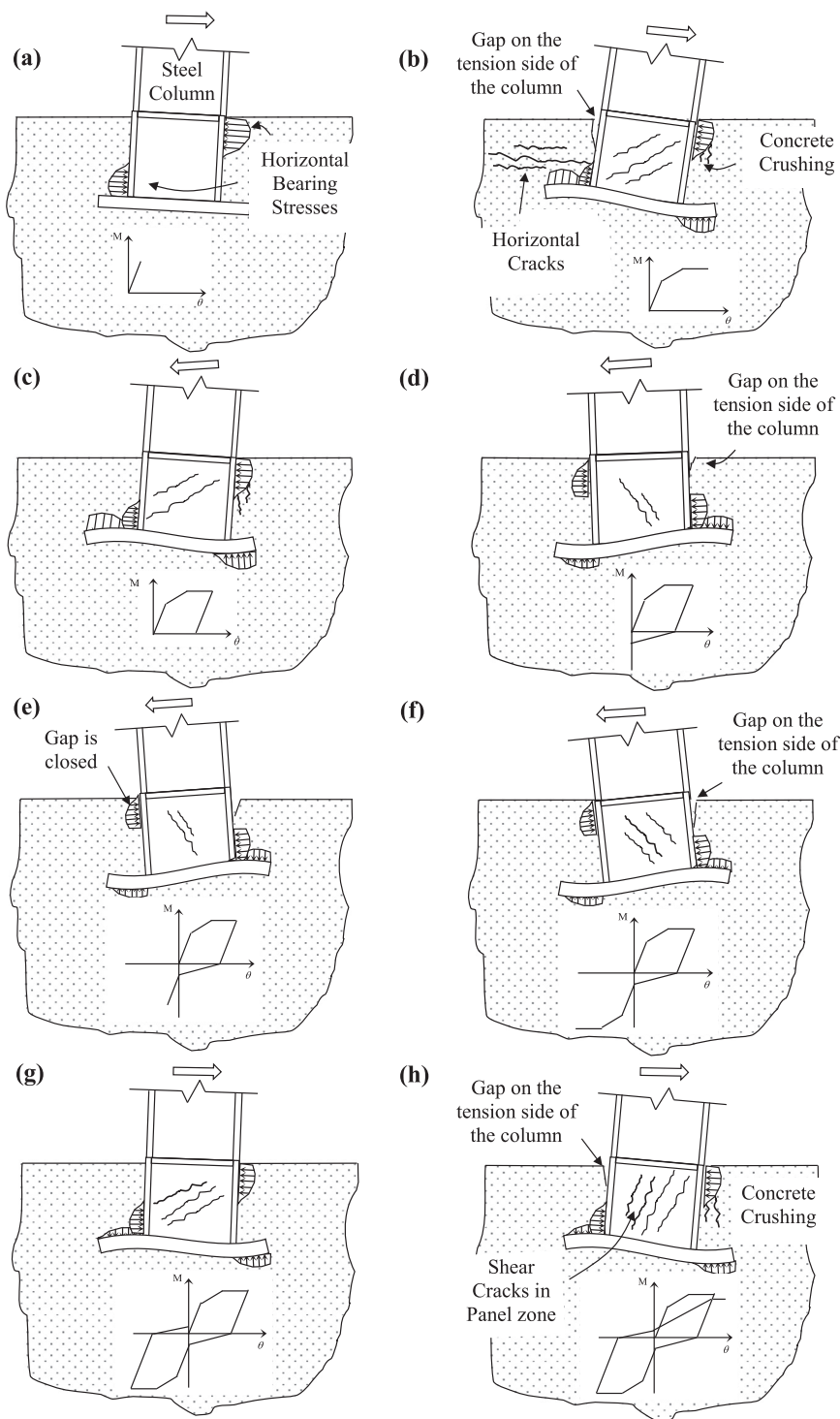


Fig. 3. Physical Response of EBC connections subjected to cyclic loading.

depth increases, accompanied by a decrease in the share carried by the vertical bearing moment, as expressed by Eqs. (3) and (4) below:

$$\alpha = 1 - (d_{embed}/d_{ref}) \geq 0 \tag{3}$$

$$d_{ref} = \frac{C}{\rho}, \text{ where } \rho = \left( \frac{E_{concrete}}{4 \times E_{steel} \times I_{column}} \right)^{1/4} \tag{4}$$

Eq. (3) implies that for embedment depths greater than  $d_{ref}$ , the embedded base plate is ineffective, and all stresses are carried by horizontal bearing. Eq. (4) (in which  $C$  is a calibration constant equal to 1.77) defines  $d_{ref}$  based on the interacting stiffnesses of the embedded

column and the surrounding concrete. Further background is provided by Grilli and Kanvinde [7]. From the standpoint of this study, the decomposition of moments in this manner is important for simulating hysteretic response, as discussed in the next section.

### 3. Hysteretic model formulation

Referring to the preceding discussion, and building on the strength model developed by Grilli and Kanvinde [7], the hysteretic response of ECB connections may be most suitably represented by two rotational springs arranged in parallel, wherein the individual springs correspond

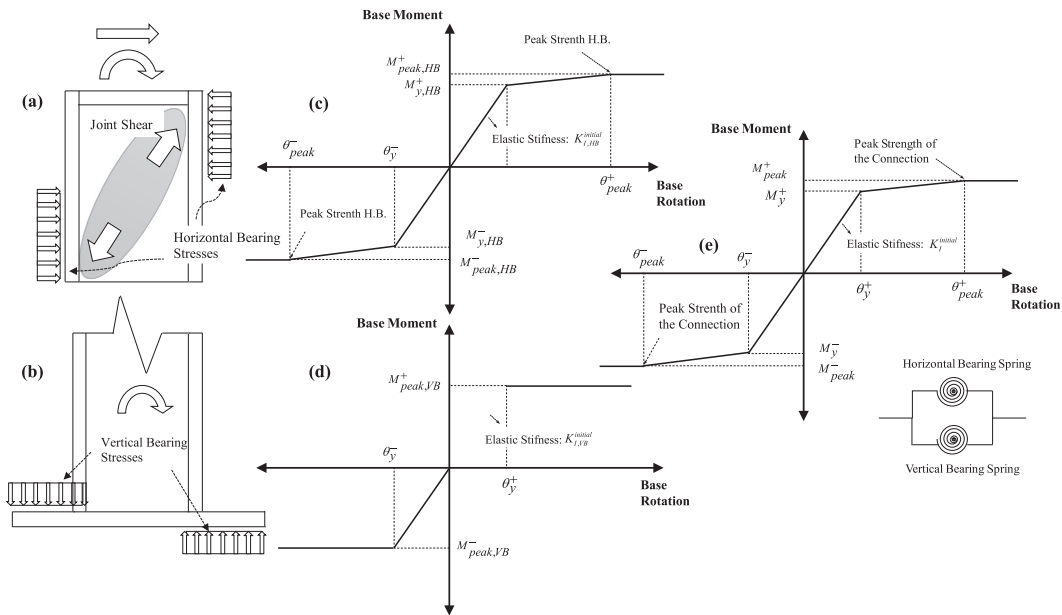


Fig. 4. Hysteretic Model Formulation: (a) Horizontal Bearing Mechanism, (b) Vertical Bearing Mechanism, (c) Backbone Curve Horizontal Spring, (d) Backbone Curve Vertical Spring, (e) Parallel Spring arrangement.

to the components of the moment carried by the horizontal and vertical bearing stresses, as outlined previously and shown in Fig. 4a and b. While the original strength model is developed to represent connection response only up to the point of monotonic failure, using its key aspects (specifically, an understanding of the internal moment distribution between the horizontal and vertical bearing mechanisms) is advantageous while simulating the hysteretic response. Specifically, the parallel springs arrangement (when used in conjunction with the hysteretic model – discussed next) successfully simulates the degradation of capacity in the horizontal bearing mechanism, and the corresponding transfer of moment to the vertical bearing mechanism. In contrast to a more simplistic approach of representing the entire connection as one hysteretic spring (as is often done – Ibarra et al. [17]), the proposed approach incorporates some degree of physical realism into the hysteretic model, with three outcomes: (1) on a purely functional basis, the model is able to represent hysteretic response with greater accuracy, due to the additional parameters associated with two springs, (2) it allows examination of moments resisted by the individual mechanisms, to assess the impact of design/detailing decisions (that impact these mechanisms independently) on hysteretic response, and perhaps most importantly, and (3) the calibration of the model parameters is more physically based, such that it is more generalizable across various configurations.

The hysteretic model developed by Ibarra et al. [17], referred to hereafter as the IMK Model (Ibarra-Medina-Krawinkler) as it is popularly known, was determined to be suitable for reproducing the physical response of ECB connections via the two-spring arrangement discussed above. The model is implemented in the platform OpenSEES [19]; simulations shown in this paper utilize this implementation. Fig. 4c–e show the spring arrangement as well as the backbone curves of the IMK model calibrated for the horizontal bearing mechanism (Fig. 4c) and the vertical bearing mechanism (Fig. 4d) within the parallel springs arrangement. For each mechanism, the backbone curve describes monotonic response, from which the cyclic hysteresis may be derived based on a set of rules. The IMK model has a trilinear backbone curve that suitably represents the first three stages of the load deformation response (see Fig. 3a-b), i.e., the linear elastic phase, hardening phase, and the plateau. For the horizontal bearing mechanism, all three branches of the backbone curve are used, with the final branch having zero slope to represent the plateau. This results in a total of four backbone parameters for the horizontal bearing spring, i.e., initial elastic stiffness  $K_{I,HB}^{initial}$ , moment at first yield  $M_{y,HB}$ , the peak (or plateau) strength  $M_{peak,HB}$ , and the rotation  $\theta_{peak}$  at which this strength is achieved. The response of the vertical bearing spring is represented through an elastic perfectly plastic backbone (since experimental data – e.g., Grilli and Kanvinde [18] does not support a more complex

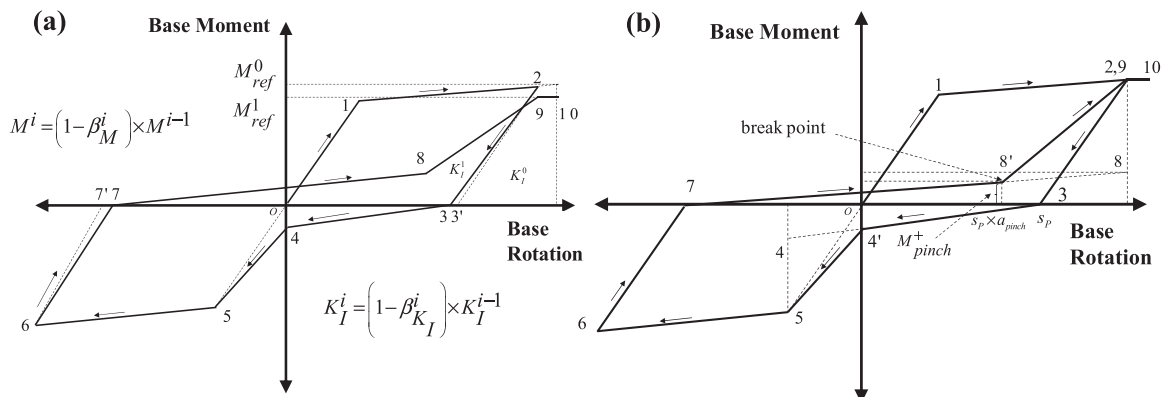


Fig. 5. (a) Hysteretic rules for pinching model, (b) Cyclic modes of deterioration.

representation); this results in two backbone parameters for the vertical bearing spring, i.e., the initial elastic stiffness  $K_{i,VB}^{initial}$  and moment at first yield  $M_{peak,VB}$ . It is important to note here that the backbone curves do not simulate a loss in strength (e.g., due to failure). This is appropriate because the IMK model backbone has three branches, and using one of them to represent softening reduces versatility with respect to modeling the “rising” portion of the moment-rotation curve. Considering the lack of data in which this type of softening is observed, using this third branch to represent the plateau (rather than softening) is a judicious tradeoff. In any case, if additional test data (showing this type of softening) becomes available, this issue may be easily addressed. Additionally, the backbone curves are assumed symmetric in both loading directions considering the common construction/design practice of ECB connections.

Fig. 5 describes the hysteretic rules which define the cyclic response as derived from the backbone, showing the stepwise evolution of the hysteretic curve for 2 cycles (where the points are numbered sequentially). This cyclic response is defined by a set of rules (and associated parameters) that are described in detail in Ibarra [17]. In the context of this paper, these are only briefly described as they pertain to the simulation of ECB connections. The IMK model is well-suited for describing two important aspects of cyclic response: (1) degradation of two quantities as the component undergoes cyclic loading, i.e., the plateau strength – denoted generically as  $M_{peak}$ , and the unloading stiffness – denoted generically as  $K_T$ , and (2) pinching, during which there is an increase in stiffness within each loading cycle corresponding to the closure of cracks or (in the case of ECB connections) gaps between the column flange and concrete footing. Deterioration of generic quantities may be simulated through rules proposed by Rahnama and Krawinkler [20], which rely on the dissipated hysteretic energy. For a generic quantity  $\Gamma$  (strength, stiffness or deformation), deterioration is expressed as:

$$\Gamma_i = (1 \mp \beta_i) \times \Gamma_{i-1} \tag{5}$$

In which  $\Gamma_i$  and  $\Gamma_{i-1}$  are the values of the quantity  $\Gamma$  during cycle  $i$  and  $i - 1$  respectively. The  $\mp$  sign indicates that deterioration may be obtained by either decreasing or increasing the quantity  $\Gamma$ . For example, if  $\Gamma$  represents a displacement used to compute an effective stiffness, deterioration of the effective stiffness is achieved by increasing the displacement from cycle to cycle. The factor  $\beta_i$  may be determined as follows:

$$\beta_i = \left( \frac{E_i}{E^T - \sum_{i=1}^{i-1} E_i} \right)^c \tag{6}$$

The factor  $\beta_i$  depends on the hysteretic energy  $E_i$  dissipated during cycle  $i$ , and the parameter  $c$  defines the rate of deterioration. The “reference energy”  $E^T$  which must be expended to obtain complete deterioration is calculated as follows:

$$E^T = \Lambda \times M_y \tag{7}$$

In the above equation,  $M_y$  is the yield moment (see Fig. 4c and d), and  $\Lambda$  is a model parameter. For a given spring, deterioration may be simulated through four model parameters (two for each of the two deterioration modes shown in Fig. 5a). These are:  $c_{K_T}$ ,  $\Lambda_{K_T}$ ,  $c_{M_{peak}}$ ,  $\Lambda_{M_{peak}}$ . In addition to these deterioration parameters, the parameters  $a_{pinch}$  and  $F_{pr}$  define the pinching point, at which stiffness is regained – see Fig. 5b. Once the modeling scheme (i.e., the two-spring arrangement, and the assignment of the IMK hysteretic model to them) has been established, the next step is to estimate the model parameters.

#### 4. Estimation of model parameters

Referring to the prior discussion, the parameters for each two-spring assembly (such as shown in Fig. 4) may be classified as backbone parameters that define the monotonic response, and the cyclic deterioration parameters. This results in 10 parameters for the horizontal spring, and 2 parameters for the vertical spring (since it is modeled as non-degrading with only two branches) with a total of 12 parameters. All parameters are listed in Table 1. Deterioration of strength and stiffness (as defined by Eqs. (5) and (6), and shown in Fig. 5) is simulated only for the horizontal spring, since it is dominant in the horizontal bearing mechanism, due to spalling of concrete as shown in Fig. 3. Test data from Grilli and Kanvinde [18] do not provide evidence of such deterioration for the vertical bearing mechanism; in fact, the vertical bearing mechanism gains strength as the horizontal mechanism deteriorates.

The efficacy of the model is evaluated for two sets of calibration – in the first set, the 12 model parameters are selected to minimize error between simulated and experimentally observed moment-rotation curves. The experimental curves are obtained from tests conducted by Grilli and Kanvinde [18]. Referring to Table 2, these tests encompass a range of configurations including variations in embedment depth, column section, and axial force. Also shown in Table 2 is the coefficient  $\alpha$  (as calculated from Eq. (3)), which determines the ratio of moment

**Table 1**  
Model parameters and their calculated or calibrated values.

Type→	Backbone parameters										Hysteretic parameters						Error		
	Horizontal spring					Vertical Spring													
	Core →Parameter?		Yes		No <sup>b</sup>	Yes	Core →Parameter?		Yes		No								
Parameter→	$K_{i,HB}^{initial}$ (10 <sup>5</sup> kN m/rad)	$M_{y,HB}$ (kN m)	$\theta_{peak}$ (rad)	$M_{peak,HB}$ (kN m)	$K_{i,VB}^{initial}$ (10 <sup>5</sup> kN m/rad)	$M_{peak,VB}$ (kN m)	$a_{pinch}$	$F_{pr}$	$c_{K_T}$	$\Lambda_{K_T}$	$c_{M_{peak}}$	$\Lambda_{M_{peak}}$	$\epsilon_u$	$\epsilon_c$					
Test↓	U <sup>a</sup>	C <sup>a</sup>	U	C	U	C	U	C	U	C	U	C							
1	1.25	1.26	1319	1012	0.022	1451	1791	0.99	1.01	1049	805	0.50	0.20	1.0	0.40	1.0	0.20	0.41	0.42
2	1.94	1.28	1200	820	0.011	1303	1496	1.76	1.17	1090	749	0.35	0.30	1.0	0.40	1.0	0.08	0.34	0.35
3	2.02	2.84	2630	2100	0.024	3083	3179	0.39	0.56	517	413	0.35	0.10	1.0	0.40	1.0	0.30	0.28	0.37
4	2.28	2.90	2677	2263	0.023	3074	3423	0.45	0.57	526	444	0.40	0.10	1.0	0.40	1.0	0.70	0.25	0.28
5	2.41	2.85	2617	2125	0.019	3180	3214	0.47	0.56	514	418	0.35	0.30	1.0	0.40	1.0	0.70	0.29	0.30
Prescribed value <sup>c</sup>	N.A.	N.A.	0.02	N.A.	N.A.	N.A.	0.39	0.20	1.0	0.40	1.0	0.40	N.A.	N.A.					

<sup>a</sup> Unconstrained or Constrained Calibration.

<sup>b</sup> All non-core parameters calibrations are unconstrained.

<sup>c</sup> Average from unconstrained calibration.

**Table 2**  
Test matrix for Grilli and Kanvinde (2015) test.

Test #	Column size (bf [mm])	$d_{embed}$ (mm)	Axial compressive force $P$ (kN)	$\alpha$
1	W14 × 370 (419)	508	445	0.45
2	W18 × 311 (305)	508	445	0.48
3	W14 × 370 (419)	762	0	0.17
4	W14 × 370 (419)	762	445	0.17
5	W14 × 370 (419)	762	– 667	0.17

between the horizontal and vertical bearing mechanisms. Selecting the 12 parameters to minimize error between test and simulated response (referred to hereafter as “Unconstrained” calibration) provides the opportunity to directly examine the ability of the approach (with its associated functional form and spring arrangement) to reproduce physical behavior, without the introduction of error due to bias in strength and

stiffness characterization models. On the other hand, parameters calibrated in this way cannot be generalized to different configurations. As a result, the second calibration set is termed the “Constrained” set, where key parameters of the backbone are independently estimated from physics-based models for ECB connections. In this case, the agreement with test data is not as good as that for the Unconstrained set, but it provides an opportunity to examine model performance in a more realistic scenario (i.e., applied to situations for which test data is unavailable). The following subsections outline the methodology used for each of these calibration exercises, whereas results of these calibrations are discussed in a subsequent section.

**5. Unconstrained calibration**

An error measure (based on the work of Smith et al. [21]) is defined to objectively determine a set of parameters that show optimal agreement with test data. Specifically, the error measure  $\epsilon$  is defined as

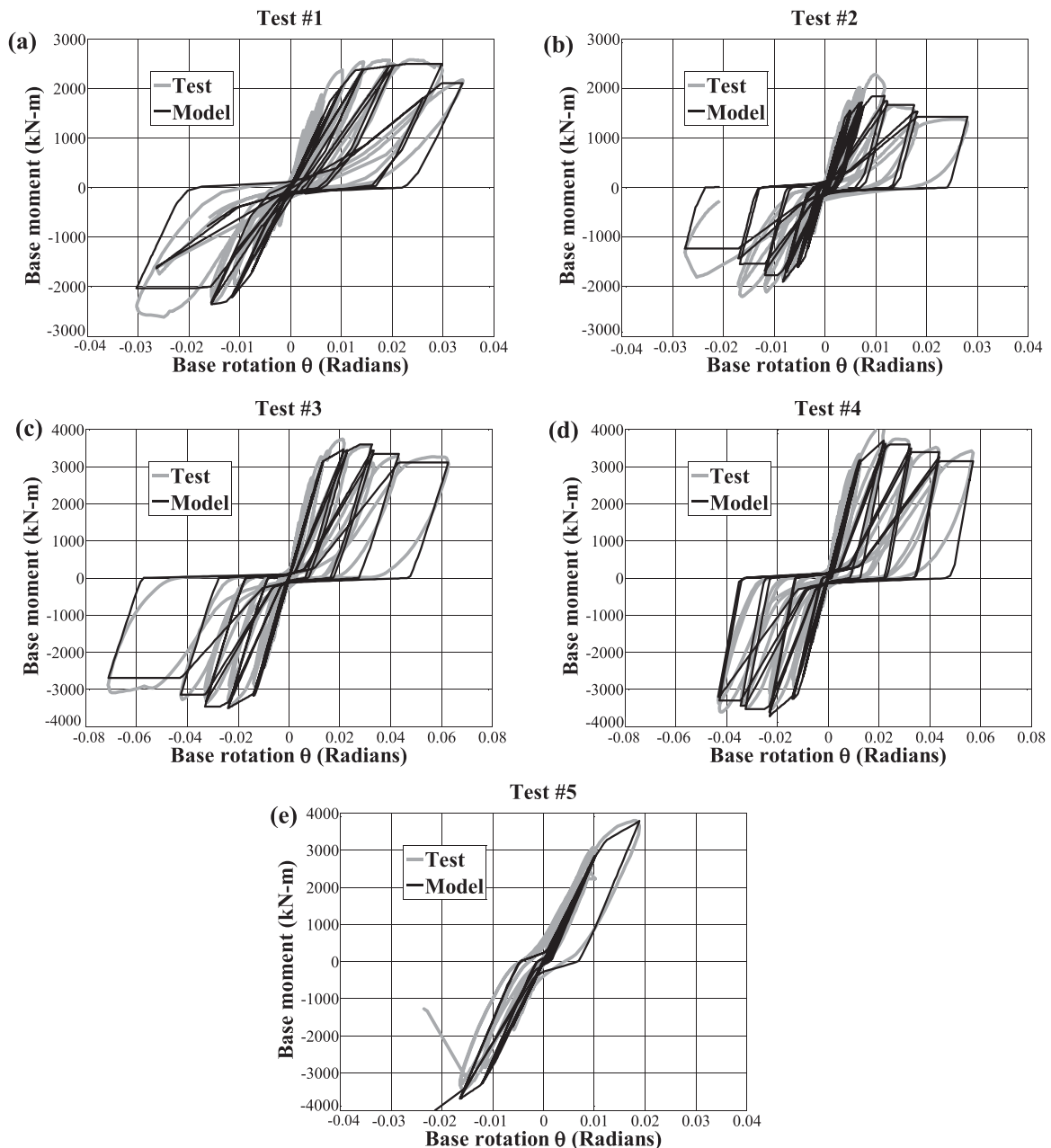


Fig. 6. Results of Unconstrained Calibration of ECB model to experimental data.

follows:

$$\epsilon = \frac{\int |M_{test} - M_{MODEL}| \cdot |d\theta|}{\int |M_{test}| \cdot |d\theta|} \quad (8)$$

The error measure is an estimate of the energy norm of the difference between the experimental moment-rotation curve and the counterpart curve obtained from the model for a given set of trial parameters. The terms  $M_{test}$  and  $M_{MODEL}$  refer to the moments obtained from the test and model at a given rotation  $\theta$ . Smith et al. [21] describe the advantages of this error measure in detail; in the context of this study, it is noted that  $\epsilon = 0$  for perfect agreement with data, and that the normalizing term  $\int |M_{test}| \cdot |d\theta|$  ensures that the error measure is not biased towards experiments with longer or shorter loading histories. For the Unconstrained calibration exercise, an optimal set of 12 parameters corresponding to the two-spring arrangement is determined. This optimal set minimizes the error  $\epsilon$  between the experimental and the model-based moment-rotation curve for that test. An automated

algorithm was developed and used for this minimization. The parameters calibrated in this manner are shown in Table 1 – the label “U” identifies parameters calibrated in an unconstrained manner.

Fig. 6a–e overlay the moment rotation curves as obtained from the calibrated model on those obtained from the test data. While results are discussed in detail in a subsequent section, a visual assessment of Fig. 6a–e indicates that the model has the functional ability to capture key aspects of response, including nonlinearity in the backbone, as well as cyclic features such as strength/stiffness degradation and pinching.

### 5.1. Constrained calibration

For this calibration exercise, five parameters are identified as “core,” which may be estimated through physics-based models developed previously. These correspond to the strength and stiffness quantities for both the horizontal and vertical bearing mechanisms. Referring to Table 1 and Fig. 4, these are  $K_{I,HB}^{initial}$ ,  $K_{I,VB}^{initial}$ ,  $M_{y,HB}$ ,  $M_{peak,HB}$ ,

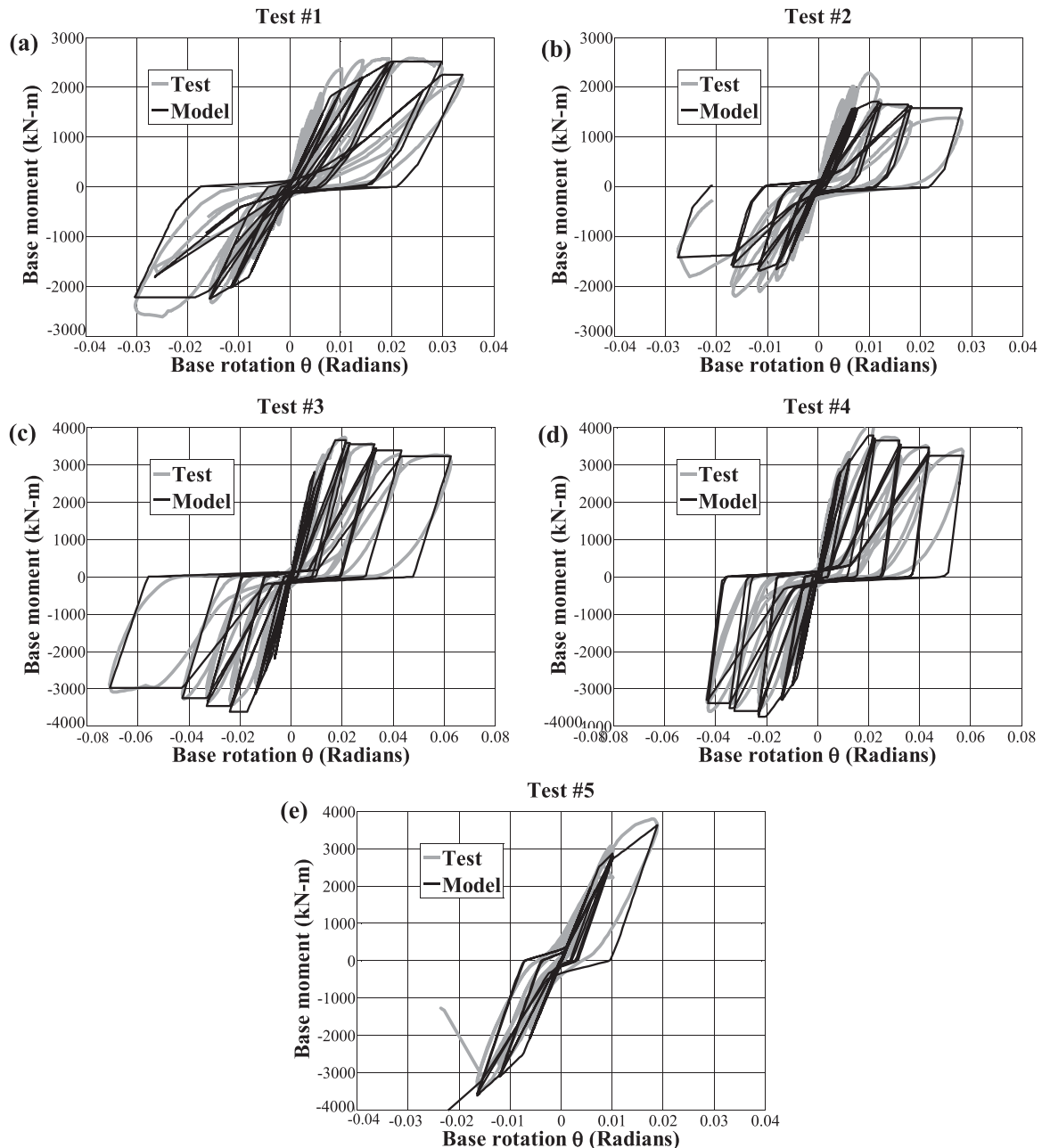


Fig. 7. Results of Calibration of ECB model after determination of core parameters.

and  $M_{peak,VB}$ . The remaining parameters (which mainly pertain to cyclic hysteresis) cannot be meaningfully determined from physics based models and must be calibrated empirically to produce agreement with test data. These are referred to as ancillary parameters. This is common practice in calibration of such hysteretic models (Ibarra et al. [17], Lignos and Krawinkler [22]). For these parameters, the values determined through the Unconstrained calibration (discussed above) are retained as the optimal fits. It is recommended that the average of these values is used for the constrained calibration (see footnote 3 in Table 1). Methods to estimate each of the core parameters are now discussed:

1. Initial stiffness values for both springs, i.e.,  $K_{I,HB}^{initial}$  and  $K_{I,VB}^{initial}$  (refer Fig. 4): Torres-Rodas et al., [10] developed a method to calculate the rotational stiffness of ECB connections. The method is based on decomposing the net base moment  $M_{base}$  into its components  $M_{VB} = \alpha \times M_{base}$  resisted by vertical bearing, and  $M^{HB} = (1 - \alpha) \times M_{base}$  resisted by horizontal bearing, and then calculating the deformations associated each mode of resistance. The approach follows a straightforward procedure to determine the net rotational stiffness of the base connection, termed  $K_I^{initial}$ , a detailed description of this procedure is presented in Torres-Rodas [10], and excluded here for brevity. The initial stiffness  $K_I^{initial}$  determined as per this procedure reflects the stiffness corresponding to the entire connection, which must be decomposed into the stiffnesses corresponding to the vertical and horizontal bearing mechanisms for the purposes of defining properties of the individual springs within the assembly. The parameter  $\alpha$  provides a means for performing this decomposition (following its interpretation as a distribution parameter for the moments), such that the initial stiffness for the two springs may be determined as  $K_{I,VB}^{initial} = \alpha K_I^{initial}$ , and  $K_{I,HB}^{initial} = (1 - \alpha) K_I^{initial}$ , in which  $\alpha$  is determined from Eqs. (3) and (4) based on connection configuration.
2. Strength values for both springs, i.e.,  $M_{y,HB}$ ,  $M_{peak,HB}$ , and  $M_{peak,VB}$  (refer Fig. 4): Grilli and Kanvinde [7] provide a method to estimate the peak strength, based on a consideration of numerous limit states including concrete crushing ahead of the column flange, panel zone failure, or uplift/blowout of concrete on the tension side of the connection due to vertical forces exerted by the embedded base plate. Briefly, the process entails the following steps: (1) determine the parameter  $\alpha$  based on the embedment depth and the properties of the column and the concrete, (2) use the parameter  $\alpha$  to distribute the applied base moment between the horizontal and vertical bearing mechanisms, (3) for each of these mechanisms, determine the critical failure mode; for the horizontal bearing mechanism, this failure mode may correspond to two limit states: a) concrete crushing ahead of the column flange, or b) Shear failure of the panel zone that is comprised of embedded column web and surrounding concrete. The moment capacity is controlled by the minimum of the moment associate to bearing failure and shear failure of the joint panel, depending on the design configuration; whereas for the vertical bearing mechanism, the failure mode may correspond to blowout of concrete either above the tension side of the embedded base plate, or under the compression toe of the embedded base plate, depending on configuration, (4) compute the strengths associated with these failure modes, and (5) determine the net strength of the connection based on these mechanism strengths combined appropriately. Grilli and Kanvinde [7] describe this process in detail. The peak strength  $M_{peak}$  for the base connection is determined through this process, and further apportioned to each of the springs such that  $M_{peak,VB} = \alpha M_{peak}$ , and  $M_{peak,HB} = (1 - \alpha) M_{peak}$ . Further, the yield moment for the horizontal spring is determined as 70% of the peak moment; this follows experimental observations by Grilli et al., [7]. Consequently,  $M_{y,HB} = 0.7 M_{peak,HB}$ . It is important to point out that test observations, and therefore the available analytical models, to determine the strength and stiffness of ECB connections are insensitive to the level of axial load.

Table 1 shows the values of the core and ancillary parameters estimated in this way. Fig. 7a–e overlay the moment-rotation curves as calibrated from the Constrained calibration over the corresponding experimental curves. Results are discussed in the next section.

## 6. Evaluation of the ECB hysteretic model against experimental data

With reference to Fig. 6a through 6e (which show the Unconstrained calibration), and Table 1, the following observations may be made about the proposed approach:

1. The two-spring arrangement (with the IMK hysteretic model) is able to reproduce experimental response with high fidelity, capturing relevant modes of behavior, including nonlinear hardening, pinching, and strength and stiffness degradation. Table 1 also summarizes the normalized error  $\epsilon$  (see Eq. (8)) between the tests and simulations, which is in the range of 0.25–0.41 (average 0.31). In itself, this may be considered an acceptable value of error, especially when evaluated relative to commonly used hysteretic models. The implication is that if the parameters are calibrated correctly, the proposed approach (i.e., combination of hysteretic models with the two-spring arrangement) is suitable for simulating the response of embedded column bases.
2. Although the overall agreement between test and simulation appears reasonable, it is noted that the hysteretic model is not able to effectively capture the nonlinearity during unloading response – since the functional form does not allow the change of slope during this region (but only after zero moment is reached upon unloading). Although a minor issue, it may result in erroneous estimates of residual rotation. Using a functional form with a nonlinear unloading branch may mitigate this problem and significantly reduce error.
3. With the exception of Test #5 (in which premature failure was noted), the error is relatively uniform across the other specimens.
4. A sensitivity analysis was conducted to examine the influence of each core parameter on the error; specifically, this analysis involved varying the parameters by  $\pm 10\%$  and noting the corresponding change in error. The sensitivities (ranked from most sensitivity observed in error to least) are as follows:  $M_{peak,VB}$  (variation in error = 6.4%),  $K_{I,HB}^{initial}$  (4.8%),  $M_{y,HB}$  (4.4%),  $M_{peak,HB}$  (0.67%), and  $K_{I,VB}^{initial}$  (0.04%). An implication of this is that the parameters with the least sensitivity are also the most challenging to calibrate directly from test data.

Fig. 7a–e show simulation results (moment-rotation plots) as determined from the constrained calibration overlaid on the test data. These may be considered representative of expected implementations for connections in buildings for which test data is not available, implying that the core parameters must be estimated, rather than calibrated (as in for the unconstrained set). As discussed earlier, the same values of ancillary parameters (summarized in Table 1) are used for the constrained and unconstrained sets. Referring to Fig. 7a–e, and Table 1, the following observations may be made.

1. Qualitatively, the model captures all modes of response observed in the experiments, in a manner similar to that shown in Fig. 6a–e for the unconstrained fit. However, in a quantitative sense, the agreement is slightly poorer, such that the error  $\epsilon$  is in the range of 0.28–0.42 (average 0.34). This is not surprising, since the core parameters are not selected freely to minimize this error, but rather calculated. As a result, the increased error is an artifact of bias in the strength and stiffness estimation models, rather than the hysteretic functional form.
2. Notwithstanding the slightly poorer fit, the error (and the associated fit) is comparable to that from the unconstrained fit. This is

encouraging from the standpoint of simulating base connections, in which the key properties (strength/stiffness) are unknown and must be estimated using models.

In summary, the two-spring arrangement with the hysteretic models is an effective approach to characterize the dissipative response of ECB connections. In terms of parameter calibrations, the use of previously developed models is appropriate for estimating the core parameters of strength and stiffness, whereas the other (ancillary parameters) must be estimated empirically. Table 1 provides such empirically calibrated estimates for use in nonlinear time history simulations.

## 7. Summary, recommendations, and limitations

This paper presents an approach to simulate the hysteretic response of embedded column base (ECB) connections that are commonly used to connect columns in Steel Moment Frames to concrete footings. Conventionally, these are designed to remain elastic during seismic shaking – this is because as connections, they are implicitly assumed to be less ductile than the adjoining column. As a consequence, previous research has focused mainly on their elastic stiffness and yield strength. However, recent work indicates that these connections may be highly ductile and disregarding their deformation capacity in design results in expensive detailing, which is required to make them stronger than the column. However, no modeling approaches are available to simulate the post-yield dissipative or hysteretic response. As a result, the response of frames with dissipative ECB connections cannot be investigated with confidence. This hinders performance assessment of such frames, ultimately precluding the development of design guidance. Motivated by this, the paper presents a method to simulate the hysteretic response of ECB connections, along with guidelines to calibrate the requisite parameters.

The proposed method seeks to directly represent physical mechanisms that control ECB response to enable more meaningful interpretations (and generalization) of estimated parameters. To this end, the paper describes various aspects of the cyclic hysteretic response of ECB connections. Many of these aspects (yielding, strength/stiffness deterioration, and pinching) are similar to those observed in other structural components. Consequently, a popular hysteretic model (the Ibarra-Medina-Krawinkler, or IMK model – Ibarra et al. [17]) is adopted to represent ECB response. Following previous experimental and strength models, the hysteretic response is decomposed into its components resulting from horizontal and vertical bearing mechanisms within the connection. As a result, the proposed model consists of two rotational springs arranged in parallel, each representing one mechanism. This results in a total of 12 parameters, which are further classified as core or ancillary parameters. The core parameters have the most pronounced effect on hysteretic response, and also represent important physical quantities, which may be estimated directly from the connection configuration using strength or stiffness models. The ancillary parameters cannot be associated conveniently (in a physics-based manner) with connection configurations. These are calibrated in an empirical manner through error minimization between the moment-rotation curves obtained through experiments and simulation.

The proposed approach is assessed against five experiments on embedded base connections. The first stage of this assessment entails calibrating all parameters in an unconstrained sense, as to minimize the error between tests and simulations. This directly examines the efficacy of the IMK model along with the two-spring arrangement to simulate hysteretic response in a functional sense. This assessment indicates that the presented approach can successfully simulate critical aspects of the hysteretic response of ECB connections. While this exercise provides a sense of the efficacy of the model functional form, parameters calibrated in this way cannot be generalized to other configurations. Consequently a “constrained” calibration is conducted, which entails estimating the core parameters (i.e., strength and stiffness for the

springs) through physics based models published previously, supplemented by ancillary parameters calibrated in an unconstrained/empirical way. The constrained calibration represents the degree of agreement with true response that may be realistically expected when the strength/stiffness of the connection are not known *a priori* and must be estimated independently (as would be the case in practical settings). This does not introduce significant errors in the simulations, other than those due to the bias in the strength/stiffness models themselves.

Based on this assessment, the proposed approach is determined to be suitable for simulating the dissipative/hysteretic response of ECB connections in steel moment frames. It is recommended (for design or performance assessment) that the core parameters be estimated through the strength and stiffness models, whereas prescribed values (as shown in Table 1) be used for the ancillary parameters.

Possibly being the first attempt to simulate the hysteretic response of ECB connections, the model has numerous limitations. These must be considered when applying the approach, as well as in interpreting results of nonlinear time history simulations that employ the approach. First, the model is validated against only five tests – since these are the only ones on deeply embedded column bases available in literature. As a result, the model inherits limitations of the testing program – e.g., the lack of significant reinforcement in the footing, and two embedment depths. Additionally, the approach recommends calibration of the third branch of the backbone as a plateau, with the implication that it does not simulate the loss of strength (i.e., failure) in the connection; this follows the observation in that a majority of tests, loss of strength was not observed – making it difficult to generalize. This may be readily addressed by prescribing a negative slope for the third branch of the backbone (see Fig. 3c), albeit it will limit the accuracy of the approach in simulating the rising phases of the backbone. These issues are the result of the need to balance accuracy with simplicity. It is anticipated that as more test data becomes available, and dissipative or yielding base connections are more commonly considered in design, models to simulate them will advance as well.

## Acknowledgments

The authors would like to thank The National Secretariat of Higher Education, Science, Technology, and Innovation of Ecuador (SENESCYT) whose graduate fellowship provided support for the lead author.

## References

- [1] Drake R, Elkin S. Beam-column base plate design LRFD method. *Eng J* 1999;36:29–38.
- [2] Kanvinde A, Grilli D, Zareian F. Rotational stiffness of exposed column base connections: Experiments and analytical models. *J. Struct. Eng.* 2012;495:549–60.
- [3] Trautner C, Hutchinson T, Grosse P, Silva J. Effects of detailing on the cyclic behavior of steel baseplate connections designed to promote anchor yielding. *J Struct Eng* 2015;142(2):04015117.
- [4] Torres-Rodas P, Zareian F, Kanvinde A. Hysteretic model for exposed column–base connections. *J Struct Eng* 2016;142(12):04016137.
- [5] Fisher J, Kloiber LA. Base plate and anchor rod design. *AISC steel design guide one*. 2nd ed Chicago, IL: American Institute of Steel Construction; 2006.
- [6] Gomez I, Kanvinde A, Deierlein G. Exposed column base connections subjected to axial compression and flexure. Final Report Presented to the American Institute of Steel Construction, Chicago, IL; 2010.
- [7] Grilli D, Jones R, Kanvinde A. Seismic performance of embedded column base connections subjected to axial and lateral loads. *J Struct Eng* 2017;143(5):04017010.
- [8] Barnwell N. Experimental testing of shallow embedded connections between steel columns and concrete footings [Master's thesis]. Provo, UT: Brigham Young University; 2015.
- [9] Grilli D, Kanvinde A. Embedded column base connections subjected to seismic loads: strength model. *J Constr Steel Res* 2017;129:240–9.
- [10] Torres-Rodas P, Zareian F, Kanvinde A. Rotational stiffness of deeply embedded column–base connections. *Journal Struct Eng* 2017;143(8):04017064.
- [11] Tryon. Simple models for estimating the rotational stiffness of steel column-to-footing connections [Master's thesis]. Provo, UT: Brigham Young University; 2016.
- [12] American Institute of Steel Construction. *Seismic Design Manual*. 3rd ed. Chicago, IL: American Institute of Steel Construction; 2007.

- [13] Lignos D, Krawinkler H. A database in support of modeling of component deterioration for collapse prediction of steel frame structures. *Struct Eng Res Front* 2007;1–12.
- [14] FEMA. Recommended seismic design criteria for new steel moment frame buildings. FEMA 350 Report; 2000.
- [15] FEMA P695. Quantification of building seismic performance factors. Washington D.C: Federal Emergency Management Agency; 2009.
- [16] NEHRP. Evaluation of the FEMA P-695 methodology for quantification of building seismic performance factors. NIST GCR 10-917-8. NEHRP Consultants Joint Venture; 2010.
- [17] Ibarra L, Medina R, Krawinkler H. Hysteretic models that incorporate strength and stiffness deterioration. *Earthq Eng Struct Dyn* 2005;34(12):1489–511.
- [18] Grilli D, Kanvinde A. Embedded column base connections subjected to flexure and axial loads. Rep. 3-11. Vancouver, WA: Charles Pankow Foundation; 2015.
- [19] OpenSEES [Computer software]. Pacific Earthquake Engineering Research Center, Univ. of California, Berkeley, CA.
- [20] Rahnema M, Krawinkler H. Effects of soft soil and hysteresis model on seismic demands. Rep. No. 108, John A. Blume Earthquake Engineering Center, Stanford Univ., Stanford, CA.
- [21] Smith CM, Deierlein GG, Kanvinde AM. A stress weighted damage model for ductile fracture initiation in structural steel under cyclic loading and generalized stress states. 2014. Technical Rep. No. 187, John A. Blume Earthquake Engineering Center, Stanford Univ., Stanford, CA.
- [22] Lignos D, Krawinkler H. Deterioration modeling of steel components in support of collapse prediction of steel moment frames under earthquake loading. *J. Struct Eng* 2011;137(11):1291–302.